Vol 18 No 9, September 2009
1674-1056/2009/18(09)/3870-07

Chinese Physics B

© 2009 Chin. Phys. Soc.
and IOP Publishing Ltd

Monte Carlo simulation of electron beam air plasma characteristics

Deng Yong-Feng(邓永锋)[a)b)†], Han Xian-Wei(韩先伟)[a)], and Tan Chang(谭 畅)[a)]

[a)] *Shaanxi Power Machine Design and Research Institute, Xi'an 710100, China*
[b)] *State Key Laboratory of Materials Modification By Laser, Ion and Electron Beams, Department of Physics, Dalian University of Technology, Dalian 116085, China*

(Received 27 September 2008; revised manuscript received 10 April 2009)

A high-energy electron beam generator is used to generate a plasma in atmosphere. Based on a Monte Carlo toolkit named GEANT4, a model including complete physics processes is established to simulate the passage of the electron beam in air. Based on the model, the characteristics of the electron beam air plasma are calculated. The energy distribution of beam electrons (BEs) indicates that high-energy electrons almost reside in the centre region of the beam, but low-energy electrons always live in the fringe area. The energy deposition is calculated in two cases, i.e., with and without secondary electrons (SEs). Analysis indicates that the energy deposition of SEs accounts for a large part of the total energy deposition. The results of the energy spectrum show that the electrons in the inlet layer of the low-pressure chamber (LPC) are monoenergetic, but the energy spectrum of the electrons in the outlet layer is not pure. The SEs are largely generated at the outlet of the LPC. Moreover, both the energy distribution of BEs and the magnitude of the density of SEs are closely related to the pressure of LPC. Thus, a conclusion is drawn that a low magnitude of LPC pressure is helpful for reducing the energy loss in the LPC and also useful for greatly increasing the secondary electron density in dense air.

Keywords: electron beam, discharge, plasma simulation, Geant4
PACC: 4180D, 5280, 5265

1. Introduction

Generating a large volume of air plasmas at atmospheric pressure is an extremely challenging research field, because it needs a particularly high power to break down the gas, during which it might cause instability problems. During the past decades, much work have been devoted to the achievement of atmospheric air plasma by traditional methods, such as DC discharge,[1] pulse discharge,[2] and the dielectric barrier discharge.[3] Nevertheless, the generating device, using the traditional method, needs special electrode geometry, which makes the discharge system complex. Additionally, in these methods, the power budget is closely related to the gas pressure.[4] In some applications, it is required that the discharge power budget should not be related to the varying pressure, and also the discharge device should be as simple as possible. In this regard, a high-energy electron beam generator is a best choice to fulfil the critical requirements.[5] By this means, the primary electrons are generated from a thermal cathode and then are accelerated to a high-energy level by a multi-anode under vacuum conditions (about 1.33×10^{-3} Pa). Then the beams of energetic electrons propagate into the atmospheric dense air through the multi-level vacuum differential pumping section. Subsequently, the high-energy BEs collide drastically with the air molecules, resulting in an electron ionization avalanche. In this process, about 30–50% of the beam energy is spent directly on the ionization of air molecules, which is three orders of magnitude higher than that of the traditional method,[6] behaving as an efficient ionization source. Therefore, it is widely adopted in some special applications, such as controlling supersonic flow by magnetohydrodynamic (MHD) means,[7] reflection and absorption of electromagnetic waves.[8]

Since most of the applications are designed to work at high pressures, there will be some undesirable problems, e.g., high recombination rate, which would greatly reduce the electron density. Moreover, even if the power budget of the electron beam source hardly depends on the gas pressure, the sustaining power is still considerably high. In 2002, Palm *et al* [9] investigated experimentally the concept of using nonequilibrium vibrational excitation to enhance the electron

†Corresponding author. E-mail: yfdeng@mail.nwpu.edu.cn

beam ionization. By this means, the power required to sustain a stable plasma was reduced; however, the device becomes more complex to some extent. In 2006, Li *et al* [10] employed a four species one-dimensional model to simulate the properties of an electron beam. The results indicated that the ionization is closely related to the beam energy, which is responsible for the density of the beam plasma. Therefore, in order to interpret the physics of the ionization clearly, it is significant to investigate the energy distribution of BEs. In Ref.[11], Soloviev *et al* developed a Monte Carlo model to simulate the spatial distribution of input power to air from a single stationary needle-like electron beam. The results indicated that input power distribution is extremely non-uniform and at the beam exit the power deposition is much higher than that at a distance away around, one half of the electron range. Similar work was done by Sheikin and Sukhomlinov in 2006.[12] The spatial distribution of the electron beam energy deposition was researched sufficiently by employing both analytical and Monte Carlo methods.

In Refs.[11]–[14], the characteristics of beam energy in some specific applications were studied in detail. However, some assumptions are made in the model, such as neglecting electron bremsstrahlung, etc. In the present paper, the analysis of electron beam air plasma characteristics is performed by a Monte Carlo model. Unlike the geometry given in the literature, we use two special chambers, i.e., a vacuum chamber and LPC, placed between the electron gun and the atmospheric dense air region (ADAR), acting as a differential pumping section. The beam energy and energy deposition are analysed in both LPC and ADAR. The influence of the pressure of the LPC on the electron beam plasma is to be investigated.

2. Simulation setup

The simulation in this paper is based on a Monte Carlo toolkit named GEANT4 (GEometry ANd Tracking), which was developed by an international collaboration.[15,16] GEANT4 is a free software package written in C^{++} which can be used to accurately simulate the passage of particles through matter. Now it is widely adopted in high energy physics, space science, and medical fields. When the user comes to his specific application, he needs to construct the detector-geometry, specify the physics-list, and generate a primary-event. Moreover, in order to extract the information of interest, the user is asked to construct other GEANT4 user-action modules.

As mentioned above, the detector geometry in this work is a cylindrical tube divided into two segments (see Fig.1): one is a vacuum chamber positioned at the exit of electron gun; the other is an LPC placed next to the vacuum chamber. Considering the complexity of the interactions between the energetic BEs and air molecules, a so-called standard electro-magnetic physics model is built, which contains all the possible processes, such as electron ionization, bremsstrahlung, multiple-scattering, and the photo-electric effect, etc.

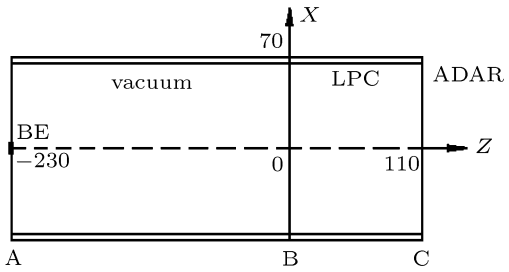


Fig.1. Schematic of the detector geometry. AB: the vacuum chamber; BC: the low pressure chamber; ADAR denotes the atmospheric dense air region. The unit of length is mm.

A more detailed description of the model is listed in Table 1. When the high-energy BEs propagate into the ADAR, according to their energy range, some proper processes are activated. If the electron energy exceeds the ionization threshold, amounts of SEs are generated, then each of them is tracked by GEANT4 automatically. In GEANT4, the ionization process is described by the G4eIonisation module. Although radiative intensity is not obviously observed in a few hundred keV, the electron bremsstrahlung process, described by G4eBremsstrahlung, is still considered in the present work, because x-ray radiation is significant in some special applications.

After the establishment of the GEANT4 physics-list module, the primary-event module also needs to be constructed. So in this C^{++} class, a virtual electron gun is established, and the initial beam energy is set at 100 keV. For the 4 mm diameter beam we are interested in, the initial positions of primary BEs are sampled within a 4 mm diameter circle and the direction of momentum is set to be the positive z direction.

Additionally, as addressed above, some optional GEANT4 user-action modules, e.g., stepping-action, event-action, and run-action, described by the corresponding C^{++} classes, are instanced to extract the

necessary information. By manipulating these user-action classes, any information can be obtained during the Monte Carlo simulation. Moreover, electro-magnetic model options and the step limit are selected to optimize the simulation.

Table 1. The physics processes described by the standard electro-magnetic model.

particle	physics process	GEANT4 module
Gamma	photoelectric effect	G4PhotoElectricEffect
	Compton scattering	G4ComptonScattering
	pair production	G4GammaConversion
e^-	multiple scattering	G4MultipleScattering
	ionization	G4eIonisation
	Moller–Bhabha scattering	G4MollerBhabhaModel
	bremsstrahlung	G4eBremsstrahlung
e^+	multiple scattering	G4MultipleScattering
	ionization	G4eIonisation
	Moller–Bhabha scattering	G4MollerBhabhaModel
	bremsstrahlung	G4eBremsstrahlung
	positron annihilation	G4eplusAnnihilation
ion	multiple scattering	G4MultipleScattering
	ionization	G4hIonisation

3. Results and discussion

3.1. Model validation

To validate the Monte Carlo model established in Section 2, the material in the LPC is replaced by graphite. Thus the high-energy BEs first propagate through the vacuum, and then get into the graphite immediately. In the GEANT4 simulation, 10^5 primary BEs are generated. By tracking the propagations of these BEs in the graphite, the energy deposition of each electron is recorded in every simulation step. In Fig.2, the simulation results of energy deposition in unit penetration depth are compared with the available numerical and experimental results given in the literature. The comparison indicates that a good agreement is achieved between our results and those of Tabata *et al*,[17] and also shows that our results agree with those of Leger *et al* [18] in general.

Both of the comparisons mean that the Monte Carlo model used in the present work is reasonable and can be applied to the calculation of the transport properties of high-energy BEs in atmospheric air.

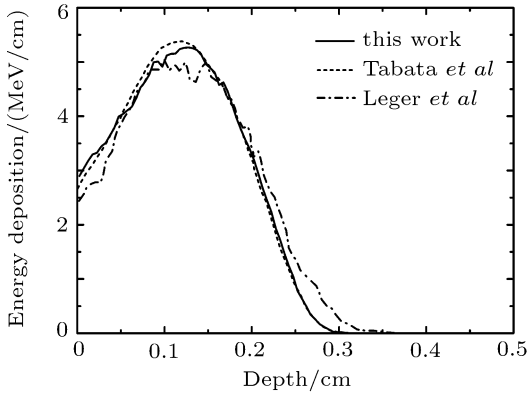


Fig.2. Energy deposition of a 1 MeV electron beam penetrating into graphite.

3.2. Beam plasma characteristics

In this section, by using the Monte Carlo model, the characteristics of the electron beam air plasma are calculated in detail. In order to analyse the results, the discharge domain is divided into regular grids. In this situation, according to the positions of electrons, the calculated data is accumulated in the corresponding grid, and then is averaged at the end of a RUN (the biggest GEANT4 simulation cycle). In the present

work, the total number of events is set at 5×10^6, i.e., 5×10^6 primary BEs are tracked.

As mentioned in the introduction, the beam plasma is generated during the collisions of energetic BEs with the air molecules. First, the BEs go through the vacuum region with hardly any energy loss, and then are injected into the LPC. After passing through the LPC, BEs penetrate into the ADAR. In Fig.3, the spatial distribution of beam electron energy is depicted. The origin of the z axis represents the inlet of the LPC and $z = 110$ mm denotes the outlet of the LPC. The results show that the beam energy is high at the inlet, where the electrons are hardly scattered, since the collision cross section is small in the high-energy range. As the penetration depth increases, the collision frequency between the BEs and air molecules becomes much higher, leading to obvious scattering of BEs. As a result, the beam electron energy is reduced; however, as seen in Fig.3, the scattered BEs are almost in the low-energy range. In contrast, the electrons in the centre region are of high energy. Therefore, such an energy distribution guarantees that a large percentage of BEs can be injected into ADAR and results in remarkable ionization.

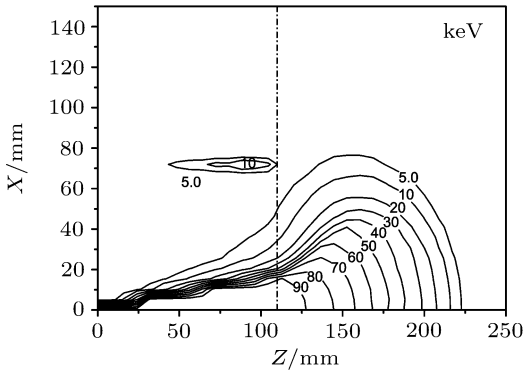


Fig.3. Spatial distribution of the beam electron energy in air. The dot-dashed line denotes the position of the outlet of the LPC.

In ADAR, due to the suddenly increased air pressure, the number density of air molecules increases sharply. The suddenly changed environment induces drastic collisions between BEs and air molecules, so that the beam radius increases exponentially. In the meantime, the beam energy decreases in both radial and longitudinal directions. Note that energy is the decisive property of BEs. Thus the spatial distribution of beam electron energy reflects the beam plasma shape to some extent. As shown in Fig.3, the beam gets its maximum radial dimension at $z = 160$ mm approximately. Subsequently, the beam tends to shrink in the radial dimension, but to increase in the z direction. Eventually, a pear shaped electron beam plasma is formed in the space.

The results also demonstrate that a low-energy region exists near the wall of LPC. It means that part of the BEs arrive at the chamber wall and deposit their energies, which could lead to extra heating of the wall of the LPC. This is a potentially uncertain factor for the safety of the electron beam generator device, which could result in the disability of the LPC. So a material of high melting point should be used to make the wall avoid ablation.

In order to illustrate BE behaviour completely, the energy deposition versus the penetration depth in two cases is shown in Fig.4. Since the SEs are generated as the electron beam propagates in air, and are also tracked to zero energy range like BEs, the energy deposition of SEs contributes to the total energy deposition at a considerably high level. Thus, the energy deposition is analysed for two cases: with and without SEs. In the case without SEs, the deposition of energy is caused only by BEs. As is observed from the profile (dashed line), the magnitude of energy deposition is small in the LPC, but it increases sharply in ADAR. The maximum energy deposition is obtained at about $z = 160$ mm, which is also the position where the beam attains its maximum radial dimension. In the case with SEs (solid line), all electrons in the discharge domain contribute to the total energy deposition. Thus, a great increase is observed in the two profiles in ADAR, but they almost overlap each other in the LPC. This is because the amount of SEs is large in ADAR, whereas it is small in the LPC.

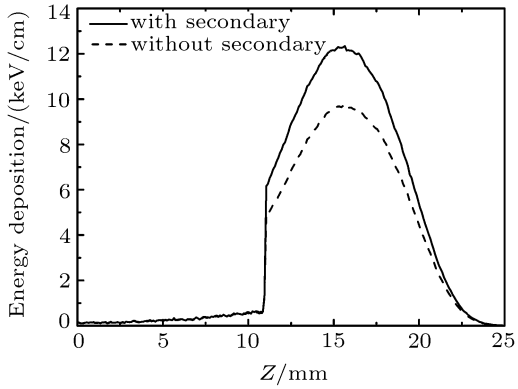


Fig.4. Energy deposition vs penetration depth in the cases with and without secondary electrons.

In the above discussions, the properties of electron energy and energy deposition are obtained by using the statistical method, which would neglect the

energy difference between electrons. In fact, the electrons are distinguished in energy from one another. Therefore, the energy spectra of BEs are analysed in two fixed layers, i.e., the inlet layer and the outlet layer of the LPC. The density is given in the scale of the maximum number density in the corresponding layer. Figure 5(a) shows the energy spectrum in the inlet layer of the LPC. It is observed that a large number of electrons have high energy, e.g., 100 keV, indicating that electrons hardly lose their energy under the vacuum condition. Figure 5(b) gives the result in the outlet layer of the LPC. The electrons are found in both high and low energy ranges. This explains the fact that some of the electrons lose their energy via collisions in LPC; however, a large part of them still have high energy, ensuring their ionization ability in ADAR.

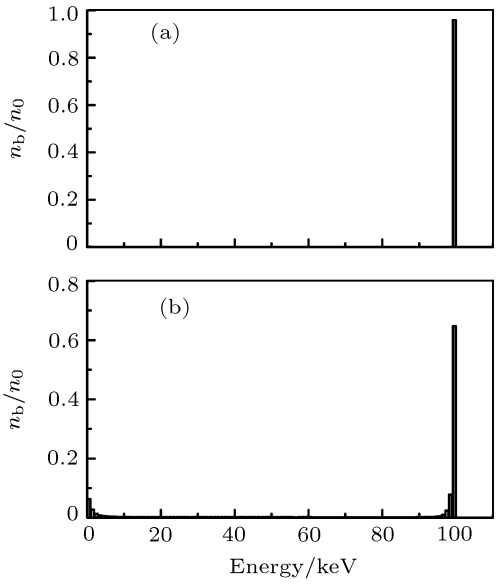


Fig.5. Energy spectra of beam electrons in (a) the LPC inlet layer; and (b) the LPC outlet layer. n_b and n_0 denote the number density of beam electrons and number density of primary beam electrons, respectively.

When the BEs are injected into the dense air, ionization is the most probable physical process to occur. If the energy of BEs exceeds the ionization threshold, the SEs are generated during the inelastic collisions between BEs and air molecules, by which a so-called electron beam plasma is formed. Figure 6 depicts the spatial distribution of SEs. The results are obtained by accumulating the number of SEs in each grid cell during a RUN. Thus the density of SEs is closely related to the number of primarily injected BEs in a simulation. So the results shown in Fig.6 are obtained in a qualitative analysis rather than a quantitative one. The results indicate that the spatial distribution of SEs is extremely non-uniform. In the LPC, the SEs are mainly generated near the centre region, and the magnitude of their density in the inlet region is larger than that in other regions. This is because the primary BEs have not been scattered yet, which leads to ionization occurring locally. Due to the low air density in the LPC, the amount of SEs is small. When BEs penetrate into ADAR, a considerably large amount of SEs is generated in the LPC outlet region. Its magnitude is six times that in the LPC, but the spatial dimension is very limited.

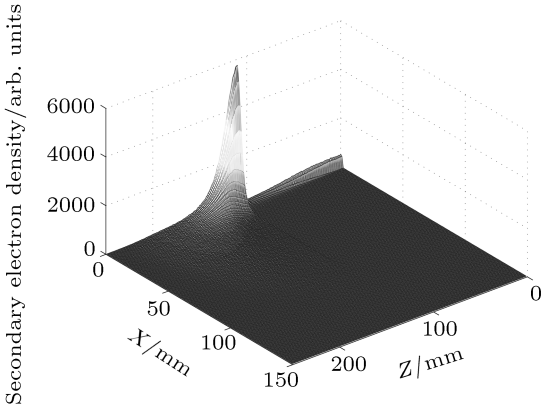


Fig.6. Spatial distribution of secondary electron density.

Furthermore, the SEs of high-energy are able to ionize the air molecules, which results in electron avalanches. The energy distribution of SEs is shown in Fig.7. By comparing with the results shown in Fig.6, it is found that the magnitude of secondary electron energy in the low density region is on the order of a few hundred eV. In contrast, the SEs in the high density region also have high mean energy. This means that on the most part the SEs can ionize the air molecules continually. Therefore, a much higher plasma density can be attained in this case.

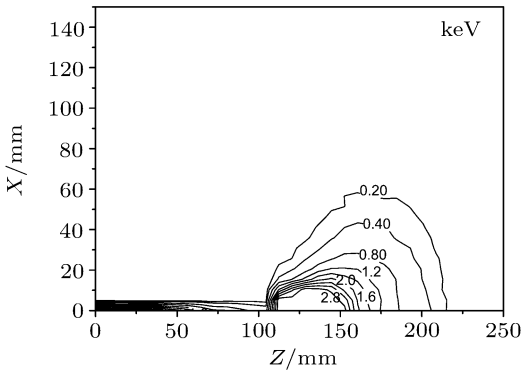


Fig.7. Spatial distribution of secondary electron energy.

3.3. Influence of LPC pressure

As stated above, an LPC is placed between the vacuum and ADAR. Thus, in this section, the influences of LPC pressure on the characteristics of beam plasma are investigated for three LPC pressure values, i.e., case 1: 1.33×10^2 Pa, case 2: 1.33×10^3 Pa, and case 3: 1.33×10^4 Pa. Note that the plasma characteristics have been examined already in detail for case 2 in subsection 3.2. Thus, the simulation here is only carried out for another two cases. Figures 8(a) and 8(b) plot the spatial distributions of beam electron energy for case 1 and case 3, respectively. For case 1, the magnitude of energy loss of BEs is little in the LPC, therefore, a great number of high-energy electrons are injected into the dense air. In contrast, the collisions become more drastic in LPC in case 3, which leads to a considerable loss of energy. Moreover, with increasing pressure of LPC, the scattering of BEs becomes serious and hence the radial dimension of the beam is enlarged. By comparing with the results shown in Fig.3, due to the large energy loss under high pressures, an obvious reduction of longitudinal range is observed with increasing LPC pressure.

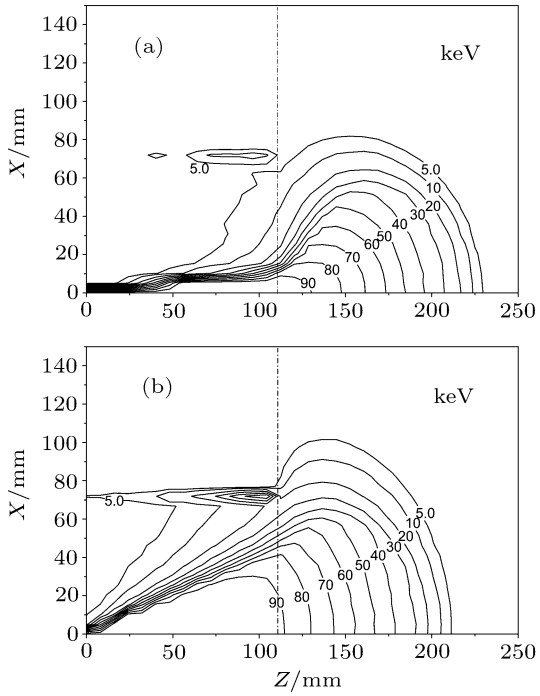


Fig.8. Spatial distribution of beam electron energy for different LPC pressures: (a) 1.33×10^2 Pa; and (b) 1.33×10^4 Pa. The dot-dashed lines denote the positions of the outlet of the LPC.

The density of SEs is also studied for three LPC pressures and the results are shown in Fig.9. As seen, in the case of 1.33×10^4 Pa, the density of SEs in LPC is much higher than that in another two cases; however, it is reduced sharply in ADAR. In contrast, in the case of 1.33×10^2 Pa, the amount of generated SEs is small in the LPC, but a sharp increase is observed in ADAR. This is because the production of SEs is determined by two factors, i.e., the number density of air molecules and the energy of BEs. In fact, the effect of the number density of air molecules is attributed to the difference of air pressures. When the LPC pressure is low, e.g., 1.33×10^2 Pa, the corresponding number density of air molecules is also small, which leads to little ionization in the LPC. Hence the density of SEs produced is low, but the energy loss of BEs is reduced, which means that considerable ionization would occur in ADAR, so the amount of SEs is large in ADAR as observed in Fig.9. By analysis, we find that to obtain a high density of plasma in ADAR and to avoid too much energy deposition at the wall of the LPC, a low pressure in the LPC is preferred.

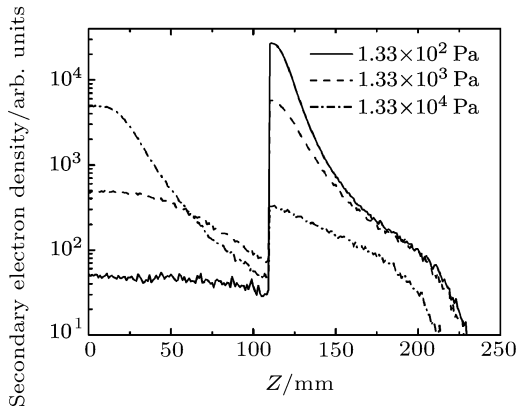


Fig.9. Secondary electron density in the axis region vs penetration depth at three different LPC pressures, i.e., 1.33×10^2 Pa, 1.33×10^3 Pa, and 1.33×10^4 Pa, respectively.

4. Conclusion

A Monte Carlo model including complete physical processes is established to simulate the passage of a high-energy electron beam in air. Based on the model, the characteristics of an electron beam air plasma are calculated. The energy distribution of BEs indicates that the high-energy electrons almost gather in the centre region of the beam, but low-energy electrons always live in the fringe area. The energy deposition is calculated for two cases, i.e., with and without SEs. The results show that the energy deposition of SEs accounts for a large part of the total energy deposition.

In order to analyse the BE energy characteristics, the energy spectrum is analysed in two layers. It can be concluded that the electrons in the inlet layer of the LPC are almost monoenergetic, but the energy spectrum of electrons in the outlet layer is not pure.

The spatial distribution of SEs shows that they are largely generated at the outlet of the LPC. The effects of LPC pressure on the properties of the beam plasma are examined. The results indicate that a low LPC pressure is helpful for reducing the energy loss in the LPC and also useful for greatly increasing the SE density in the dense air.

References

[1] Goossens O, Callebaut T, Akishev Yu, Napartovich A, Trushkin N and Leys C 2002 *IEEE Trans. Plasma Sci.* **30** 176

[2] Naidis G V 1997 *J. Phys.* D **30** 1214

[3] Choi J H, Lee T I, Han I, Baik H K, Song K M, Lim Y S and Lee E S 2006 *Plasma Source Sci. Technol.* **15** 416

[4] Deng Y F, Han X W, Rehman S U and Liu Y 2008 *Phys. Plasmas* **15** 053507

[5] Song F L, Zhang Y H, Xiang F and Chang A B 2008 *Acta Phys. Sin.* **57** 1807 (in Chinese)

[6] Adamovich I V, Rich J W, Chernukho A P and Zhdanoke S A 2000 *AIAA-Paper* 2000-2418

[7] Cipollini F and Muylaert J M 2006 *AIAA-Paper* 2006-3832

[8] Vidmar R J 1990 *IEEE Trans. Plasma Sci.* **18** 733

[9] Palm P, Plonjes E, Adamovich I V and Rich J W 2002 *AIAA-Paper* 2002-0637

[10] Li H, Su T, Ou Y L, Wang H H, Bai X Y, Chen Z P and Liu W D 2006 *Acta Phys. Sin.* **55** 3506 (in Chinese)

[11] Soloviev V R, Konchakov A M and Krivtsov V M 2001 *AIAA-Paper* 2001-3089

[12] Sheikin E G and Sukhomlinov V S 2006 *AIAA-Paper* 2006-1369

[13] Xiao P, Zhang Z M, Sun X and Ding Z J 2006 *Acta Phys. Sin.* **55** 5803 (in Chinese)

[14] Li W Q and Zhang H B 2008 *Acta Phys. Sin.* **57** 3219 (in Chinese)

[15] Agostinelli S *et al* 2003 *Nucl. Instr. and Meth.* A **506** 250

[16] Allison J *et al* 2006 *IEEE Trans. Nucl. Sci.* **53** 270

[17] Tabata T, Andreo P and Ito R 1994 *At. Data Nucl. Data Tables* **56** 105

[18] Leger J, Yousfi M, Eichwald O, Loiseau J F and Held B 2005 *J. Phys.* D **38** 10